HHS Public Access

Author manuscript

Magn Reson Med. Author manuscript; available in PMC 2015 December 28.

Published in final edited form as:

Magn Reson Med. 2011 May ; 65(5): 1437–1447. doi:10.1002/mrm.22740.

Intravoxel incoherent motion (IVIM) imaging of tumor microenvironment in Locally Advanced Breast Cancer

E. E. Sigmund[1], **G. Y. Cho**[1], **S. Kim**[1], **M. Finn**[1], **M. Moccaldi**[1], **J. H. Jensen**[1], **D. K. Sodickson**[1], **J. D. Goldberg**[2], **S. Formenti**[3], and **L. Moy**[1]

[1]Department of Radiology, New York University Langone Medical Center, New York, NY USA

[2]Division of Biostatistics, New York University Langone Medical Center, New York, NY USA

[3]Department of Radiation Oncology, New York University Langone Medical Center, New York, NY USA

Abstract

Diffusion-weighted imaging (DWI) plays important roles in cancer diagnosis, monitoring, and treatment. While most applications measure restricted diffusion by tumor cellularity, DWI is also sensitive to vascularity through the intravoxel incoherent motion (IVIM) effect. Hypervascularity can confound apparent diffusion coefficient (ADC) measurements in breast cancer. We acquired multiple b-value DWI at 3 T in a cohort of breast cancer patients and performed biexponential IVIM analysis to extract tissue diffusivity (D_t), perfusion fraction (f_p), and pseudodiffusivity (D_p). Results indicated significant differences between normal fibroglandular tissue and malignant lesions in ADC mean (± standard deviation) values (2.44± 0.30 vs. 1.34 ± 0.39 μm^2/ms, $p < 0.01$) and D_t (2.36± 0.38 vs. 1.15 ± 0.35 μm^2/ms, $p < 0.01$). Lesion DWI signals demonstrated biexponential character in comparison to monoexponential normal tissue. There is some differentiation of lesion subtypes (invasive ductal carcinoma (IDC) vs. other (OT) malignant lesions) with f_p (10.5 ± 5.0% vs. 6.9 ± 2.9%, $p = 0.06$), but less so with D_t (1.14±0.32 μm^2/ms vs. 1.18 ± 0.52 μm^2/ms, $p = 0.88$), and D_p (14.9 ± 11.4 μm^2/ms vs. 16.1 ± 5.7 μm^2/ms, $p = 0.75$). Comparison of IVIM biomarkers with contrast-enhancement suggests moderate correlations. These results suggest the potential of IVIM vascular and cellular biomarkers for initial grading, progression monitoring, or treatment assessment of breast tumors.

Keywords

diffusion; pseudo-diffusion; breast cancer; intravoxel incoherent motion; perfusion fraction

I. INTRODUCTION

Cancer in all of its forms remains one of the most lethal and incurable diseases threatening public health. The resistance of tumors to effective treatment is in part due to their diversity and microstructural complexity in both the vascular and parenchymal tissue compartments.

Corresponding author: Eric E. Sigmund, PhD, 660 First Ave., 4th Floor, New York, NY 10016, Ph: (212) 263-4841, FAX: (212) 263-4830, eric.sigmund@nyumc.org.

As such, diffusion-weighted imaging (DWI) plays an important role in characterizing the tumor microenvironment, usually to probe tumor cellularity, since the proliferation of cancer cells generally reduces the extracellular space, which in turn reduces the apparent diffusion coefficient (ADC). Changes in ADC values are observed for tumors in, e.g., the brain [1], liver [2], kidney [3], cervix [4], breast [5], and prostate [6]. Conversely, ADC measurements have been shown to increase with tumor necrosis as tumor cells are treated using radiation or chemotherapy [7-9]. Some tumors deflect (rather than infiltrate) native tissue that retains function despite its displacement; discriminating between these cases has become a powerful presurgical application of diffusion tensor imaging (DTI), where tools like fiber-tracking are used to ensure that viable tissue is not damaged during resection [10]. Recent studies have shown that even the infiltrating cellularity itself can display diffusion anisotropy [11-13]. The sensitivity of DWI to the cellular structures of cancerous tissue is well documented and has played an increasingly important role in patient management [14].

A less commonly applied aspect of DWI is its sensitivity to vascularity, since active non-Brownian water motion processes such as blood flow can contribute to apparent diffusion. Orientationally incoherent blood flow generates a “pseudo-diffusion” effect that is known as “intravoxel incoherent motion (IVIM)” [15,16]. IVIM, first described by LeBihan et.al. for brain imaging [17], is undergoing somewhat of a revival in applications throughout the body [2,18-20]. The IVIM technique has been applied in various cancer types, such as hepatic lesions [2], brain tumors [15], and animal models [21,22].

In the case of breast cancer, DWI has been employed to add quantitative characterization to the morphological assays provided by anatomical MRI. Cellularity has been probed with DWI in breast lesions via the ADC in several patient studies [23-25] and more detailed quantification of cellular compartmentation has been found in xenograft tumor models of breast cancer [26]. Treatment effects have also been measured, signifying successful delivery of cytotoxic therapy [24,25]. The role of vascularity in the DWI response of breast lesions has been recognized in several studies via a dependence of the ADC on the particular diffusion weighting factors (b) chosen in the protocol [23,27-30]. Bogner et al. [27] performed a comprehensive survey of this dependence in a large patient group and suggested sampling protocols for ADC analysis that maximized group differentiation and efficiency. Baron et al. [31] performed dense b-value sampling and fat suppression variations in breast DWI, and concluded perfusion effects did not contribute to apparent diffusion in normal fibroglandular tissue. Partridge et al.[32] explored the use of the ADC to detect malignant but mammographically occult lesions. However, a direct quantification of vascular biomarkers beyond the ADC via DWI has yet to be demonstrated in a cohort of breast cancer patients. Some malignant lesions possess both high vascularity (significant pseudodiffusion) and high cellularity (restricted passive diffusion), which oppositely influence the DWI signal decay and can thus lead to confusion within the ADC model. A compartmental analysis explicitly resolving vascular and parenchymal effects, as performed in the present study, would thus be beneficial both for avoidance of systematic error and for enhanced quantification ability.

Contrast-enhanced imaging also plays an important role in radiological workup of suspected breast lesions. Post-contrast imaging is the current standard for conclusive identification of

hypervascular and likely malignant lesions, and quantitative dynamic contrast enhanced (DCE) MRI provides a set of markers characterizing the vascular and interstitial space as well as exchange between them [25,33,34]. In particular, measures of vascular permeability —which is typically high in “leaky” tumor vasculature—have been shown to be a powerful diagnostic tool when analyzed with appropriate models [35,36]. This further underscores the crucial role of vascularity in a complete lesion characterization and suggests its inclusion in analysis of DWI data may increase its diagnostic specificity. Another important possibility is that the use of vascular biomarkers from non-contrast DWI may reduce exclusive reliance on CE-MRI when contrast agent toxicity is an issue.

Given the dire prognosis of untreated malignant lesions, the significant costs and hardship incurred during prolonged treatment pathways (chemotherapy, lumpectomy, or mastectomy), and the scarcity of resources for arbitrary screening protocols, the importance of accurate non-invasive screening or grading procedures cannot be overstated. The unique sensitivity of IVIM-MRI to simultaneous biomarkers of cellularity and vascularity underscores its value in characterizing complex cancerous tissue. The present study employs IVIM-MRI acquisition and analysis techniques in a group of patients with breast lesions at 3 T. The goal of this study is to demonstrate feasibility of measuring biomarkers of tumor cellularity, vascularity, and blood velocity in breast lesions. Such a radiological tool may enable future studies that might individually monitor the effects of treatment on each of these properties of the microenvironment.

II. Materials and Methods

A. Patient data

Thirty-four breast patients (mean age 53.1 years, range 39-85 years) were included in this IRB-approved HIPAA-compliant prospective study from the following dates: 1/7/2009-1/28/2010. All subjects had either prior suspicion or diagnosis (via mammography, MRI-guided biopsy or Fine Needle Aspiration (FNA) biopsy) of breast cancer. Among 34 patients, 45 suspicious lesions were identified : 5 pts w/ no lesions, 19 pts w/ 1 lesion, 9 pts w/ 2 lesions, 1 pt w/ 3 lesions, and 1 pt with 5 lesions. Two lesions were excluded from our analysis for lack of pathology data, leaving 43 as shown in Table 1. In 19 cases, the lesion size was too small in at least one plane (mean size 10 mm, range 8 – 15 mm) to be directly observed on DWI. DWI was successfully collected in the remaining 24 cases: 2 ductal carcinoma in-situ (DCIS), 2 invasive lobular carcinoma (ILC), 1 adenocarcinoma, and 19 invasive ductal carcinoma (IDC) lesions. Within this group, one patient had both a DCIS lesion and an IDC lesion, and another had 2 IDC lesions; the other 20 lesions were in different patients. Contrast enhancement data was available for 23 of the 24 lesions with DWI data. Final diagnosis was confirmed by histology, surgery and clinical and imaging follow-up.

B. MRI protocols

Patients were scanned in a Siemens full-body 3 T scanner (TIM Trio, Siemens, Erlangen, Germany) equipped with a 7-channel breast coil array (In Vivo, Orlando, FL), in prone position with dual breast compression. Pre-contrast anatomical imaging was performed with

fat-saturated and non fat-saturated T1 weighted volume interpolated breathhold exam (VIBE) (resolution 1.2 × 0.9 × 1.5 mm, scan time 1:10 each) sequences. Total scan time for the pre-contrast T1 VIBE scans was 2.3 minutes.

DWI scans were carried out for each patient using the pulse sequence depicted in Figure 1. Standard DWI was performed using a single-shot, twice-refocused spin echo sequence with bipolar diffusion gradients and centric ordered turbo spin echo (TSE) readout [37-39]. While most previous lower field breast DWI studies have employed echo-planar imaging (EPI) readouts, the TSE sequence was chosen here to avoid susceptibility-induced distortions that worsen at higher applied field. Axial TSE-DWI images with bilateral breast coverage were collected (TR / TE = 2000 / 103 ms, matrix 106 × 128 × 12, resolution 2.7 × 2.7 × 4 mm, echo train duration 110*4.5ms = 495 ms) with frequency-selective fat suppression and diffusion sensitization in the anterior-posterior (A-P) direction applied with weighting factors of b=0, 30, 70, 100, 150, 200, 300, 400, 500, and 800 s/mm^2. Total scan time for the TSE-DWI scan was 4 minutes. The slice group measured in the TSE-DWI scan did not achieve full breast coverage but rather were centered on the lesion of interest as identified in the anatomical scan.

Sagittal 3D T1-weighted fat-saturated VIBE images (resolution 1.4 × 0.9 × 1.5 mm) were collected just before contrast and at 5 consecutive time points (duration 1:13 each) following the administration of Gd-DTPA contrast agent (Magnevist, dosage 1 cc / 10 lbs body weight; average 14.6 ± 5.1 cc). The dynamic portion of the scan lasted between 7.5 and 10 minutes depending on patient morphology. A fat-saturated sagittal T2-weighted turbo spin echo (TSE) (resolution 1 × 1 × 5 mm) scan was performed post-contrast. Total scan time for the T2 TSE scan was 4.5 minutes An axial 3D VIBE scan (1.3 × 1.1 × 1.5 mm, scan time 1 minute) was performed for guidance in analysis of the axial DWI images.

C. Data analysis

1. Anatomical imaging and lesion sampling—Typical anatomical imaging results are shown in Figure 2. Lesions were first identified as hyperintense areas in post-contrast axial T1 VIBE images by breast radiologists (MF, LM) with 4 and 12 years of experience. Lesion characteristics of location, size, morphologic and kinetic features according to the ACR BI-RADS [40] MR lexicon were recorded. For time-dependent contrast enhancement analysis, commercially available MRI-CAD software with color-coded time-intensity mapping (DynaCAD, Invivo) was used. The readers were blinded to the histology of the suspicious lesions. The dynamic contrast-enhanced scan and DWI were reviewed independently, and reported on separate occasions. Histopathologic data was obtained for the 24 lesions in our series from ultrasound-guided FNA biopsies, MRI-guided biopsies, and/or surgical pathology. With the post-contrast axial T1 images as a reference, the lesion was located in the axial TSE-DWI images, similar to previous studies [23,24,27,31,32] Some lesions appeared hyperintense on the unweighted (b = 0) images due to T2 contrast from high fluid content. In most cases, lesion ADC values were lower than normal fibroglandular tissue (e.g. ADC < 2 μm^2/ms) and could be localized in the ADC map. The combination of post-contrast T1-weighted images and ADC analysis provided a robust means of lesion localization for further quantitative analysis with the multicompartment IVIM model. Once

the lesion was identified, a ROI was drawn on the slice with the largest tumor area enclosing the whole lesion and signals were collected from that ROI for all b-values. In 19 of the 22 patients in the final series, a region (volume > 2 cm^3) of normal fibroglandular tissue in the same DWI slice was also sampled to observe diffusion behavior in normal tissue. The remaining 3 women had sparse fibroglandular tissue or predominantly fatty breasts, and a sufficient region of normal tissue (voxel > 2 cm^3) could not be obtained. Adipose (fatty) tissue was not explicitly sampled.

The average ± standard deviation ROI size for lesions (normal tissue) (excluding the large lesion shown in Figure 6) was 24.8 ± 19.1 (16.3 ± 14.1) voxels or 1.81 ± 1.39 (1.19 ± 1.03) cm^2, corresponding to an average diameter of 1.52 ± 1.33 (1.23 ± 1.15) cm.

2. IVIM analysis of DWI—The TSE-DWI image series was first processed voxelwise with a monoexponential decay model to generate an ADC map for each acquired slice. This map was used for lesion localization to guide the IVIM ROI processing. For each ROI signal decay curve, the "segmented" IVIM analysis described below was carried out to estimate ADC values and IVIM parameters D_t, D_p, and f_p.

The model employed for the diffusion weighted magnetization M is a bicompartmental model defined by four parameters: total magnetization M_0, perfusion fraction f_p, pseudo-diffusivity D_p, and tissue diffusivity D_t:

$$M = M_0 \left(f_p \, exp\left(-bD_p\right) + \left(1 - f_p\right) exp\left(-bD_t\right)\right) \quad (1)$$

As in other *in vivo* IVIM studies [19,20,41-43], where finite data sampling/precision, small perfusion fraction and/or similar compartmental diffusivities make an unconstrained fit ill-conditioned, a more numerically stable "segmented" analysis procedure was performed as follows. Typically, D_p is significantly greater than D_t, so that when the b-value is significantly greater than ~1/D_p (e.g. for D_p ~10 μm^2/ms, b > 100 s/mm^2) the influence of the pseudodiffusion term on the signal decay is quite small. Thus, in this higher b-value regime, Eq. (1) can then be simplified into an exponential fit equation whereby D_t and f_p can be estimated:

$$M_{high} = M_0 \left(\left(1 - f_p\right) \, exp\left(-bD_t\right)\right) \quad (2)$$

Operationally, D_t is determined from such a monoexponential fit to data above a chosen threshold (in this study b > 200 s/mm^2), whose zero intercept M_{int} is used along with the unweighted (b=0) signal M_0 to determine the perfusion fraction f_p, according to

$$f_p = \frac{M_0 - M_{int}}{M_0} \quad (3)$$

With D_t and f_p values calculated by using Eq. (2), D_p values can be calculated by using a partially constrained nonlinear fit of the entire dataset to Eq. (1).

In the case of parametric map analysis, an additional step is taken (residual masking) to avoid overfitting monoexponential voxels. In each voxel, prior to IVIM analysis, a single

exponential model fit is applied to the full dataset to estimate an ADC value. If the residual of this fit does not exceed a given fiduciary value determined by the standard deviation of background image noise, then the voxel is deemed monoexponential. If the residual exceeds the noise threshold, due to systematic error of the insufficient ADC model, the IVIM analysis is performed. In the final parametric maps, monoexponential voxels' ADC values are used for diffusivities D_p and D_t to provide spatial continuity without excessive random noise.

To compare tissue types, summary statistics including means and standard deviations were computed for each diffusion parameter for the following classes: normal fibroglandular tissue n = 20), all lesions (n = 24), invasive ductal carcinoma (IDC) (n = 19), and five other (OT) malignant lesions: DCIS (n=2) and ILC (n=2), and adenocarcinoma (n=1). For each parameter, the following classes were compared: (a) between all normal and all lesions, (b) between all normal and each lesion group (IDC or OT), and (c) between IDC lesions and OT lesions. Two-sided t-tests with α=0.05 were used to evaluate the statistical significance of the observed difference. For comparisons between lesions and normal tissue in the same patients, a two-sided paired t-test was also used. Since two patients showed two lesions, a comparison of all lesions with normal tissue was also tested using the average IVIM parameters from both lesions as that patient's representation in the group. Percent differences between group average values were also computed to summarize the results. No adjustments to p–values are incorporated for multiple endpoints.

3. Contrast-enhanced imaging analysis—Lesion contrast enhancement curves were sampled from contrast-enhanced MRI over a ROI drawn enclosing the full lesion on sagittal VIBE images. The initial enhancement was estimated from the difference of the first two points, and the correlations of this value with all biomarkers derived from ADC and IVIM analysis were estimated for the whole lesion group as well as for the IDC group alone. A clinical evaluation of the kinetic contrast enhancement time series was performed using DynaCad software, in which Type 1 shows a persistently increasing kinetic curve, Type 2 shows a plateau, and Type 3 shows a washout (final decrease) response.

III. RESULTS

Among the 24 cancers in our series, 15 were morphologically classified as masses (12 IDC, 2 ILC, 1 adenocarcinoma) and 9 as non-mass-like enhancement (7 IDC, 2 DCIS). Regarding the contrast-enhancement kinetic behavior (available in 23 lesions), five lesions (1 DCIS, 4 IDC) displayed a Type 1 persistent kinetic curve, 5 IDC lesions and 1 adenocarcinoma displayed a Type 2 plateau curve, and 12 lesions (2 ILC, 1 DCIS, 9 IDC) had a Type 3 washout curve. No particular morphologic or kinetic feature was consistently seen in our IDC lesions.

Figure 3 shows exemplary images from a patient with left breast IDC. Post-contrast T1-weighted imaging shows the location and morphology of the lesion in the lateral posterior area as hyperintense compared to surrounding normal fibroglandular (FG) tissue. Diffusion-weighted images show the fibroglandular tissue; at high diffusion weighting (b = 800 s/mm^2) the lesion is distinguishably hyperintense due to restricted diffusion induced by the

tumorous cellularity. This is confirmed by a monoexponential ADC map, in which ADC values in the lesion are lower than those in surrounding fibroglandular tissue. Figure 3e shows contrast-enhancement curves from the perfusion-weighted imaging series in both the mass region and normal tissue. Enhancement is much higher in the mass region, evidencing the blood volume contribution from angiogenesis. Figure 3f shows DWI decay curves in the mass and normal tissue regions of interest for this case (Fig. 3b). The mass ROI curve shows reduced signal attenuation as well as a biexponential response in comparison to the faster, monoexponential decay of normal fibroglandular tissue.

Figure 4 shows examples from several more lesions identified in this study, including post-contrast T1 weighted images, DWI b = 0 images, ADC maps, and DWI signal decays. In each case, the lesion is hyperintense on CE-MRI and b=0 images, possesses lower ADC than surrounding fibroglandular or adipocytic tissue, and displays biexponential signal decay. Curve fitting results to the IVIM model are shown for each of the masses, and fits to a monoexponential model are shown for the normal tissue.

Figure 5 shows a correlation of perfusion fraction f_p and perfusion-weighted imaging initial enhancement for the patient group in this study. The correlation coefficients between all IVIM parameters and the initial enhancement, for the whole lesion group and the IDC subgroup, are shown in Table 2. Correlations are moderate and increase slightly when only the IDC group is considered.

Figure 6 shows a LABC case with a large metaplastic IDC lesion throughout the left breast of a patient. The morphology of this mass includes a vascular rim that enhances with contrast, a main body of aggressive cellularity, and a necrotic core. The perfusion fraction (f_p) map is nonzero only in the main cellular body and vascular rim, consistent with the elevated microvessel density in the tumor, as compared to the necrotic core or the fibroglandular tissue. The tissue diffusivity is significantly lower in the tumor mass than the necrotic area. Finally, the pseudo-diffusion coefficient D_p, defined only in regions of nonzero perfusion fraction f_p, shows values near ~10 μm^2/ms. Two-dimensional histograms were generated to illustrate the cross-correlations between the IVIM parameters in the tumor tissue for this lesion only. While the fast and slow diffusivities (D_p and D_t) show little correlation, the more broadly distributed perfusion fraction f_p shows a weak negative correlation with both diffusion parameters.

The results of IVIM analysis of all breast lesion ROI are shown in Table 3 and depicted in Figure 7. Average values and standard deviations are given for *ADC*, D_t, f_p, and D_p parameters, for the following groups: (a) normal fibroglandular tissue (FGT) (N = 20), (b) all lesions (N = 24), (c) invasive ductal carcinoma (IDC) (N =19), and (d) other (OT) malignant lesions (2 DCIS, 2 ILC, 1 adenocarcinoma) (N = 5). In Table 3, Student's t-test p-values for comparisons of group (a) with (b), group (a) with (c), and group (c) with (d) are shown along with percentage differences ($\Delta = (2*(a-b)/(a+b))*100\%$) for each tissue type.

ADC and D_t values in all cancerous lesions are found to be significantly lower than those in normal tissue ($p < 0.01$), a result that is also true for the paired t-test comparison of normal and lesion results in the same patients, and is also robust whether the two lesions from one

patient are included individually or averaged in an unpaired analysis. Percentage difference between normal and lesion group is higher for D_t than for ADC, while in normal tissue D_t and ADC are equivalent. Both ADC and D_t significantly ($p<0.05$) differentiate FGT from both OT and IDC groups, with comparable differences for IDC vs. FGT differentiation (57.7 % for ADC, 69.6% for D_t) and for OT vs. FGT (61.6 % for ADC, 66.7% for D_t). D_t values are 16.4% less than ADC values in IDC lesions ($p=0.07$). In the IDC group, f_p values are 41.4% higher ($p=0.06$) than those in OT lesions. Also, in the IDC group, average ADC values are 4.2 % higher, D_t values 3.3 % lower, and D_p values 7.5 % lower than those in OT lesions.

IV. DISCUSSION

The issue of “optimal” b-values for DWI is an important and highly studied one [27,44,45] when a monoexponential (ADC) model is employed for data analysis. Studies have shown that vascularity, tissue compartmentation, and signal-to-noise effects demand that consistent b-values be used within and between studies if meaningful comparisons are to be made [44]. Scan time practicality has led to suggestions of 1 or 2 optimal b-values for a given organ [27,45,46], whose use can increase clinical differentiation. However, with significant vascularity, the ADC model will for any sampling be an incomplete description of the tissue response and thus severely limit quantitative specificity or comparison with histology. The approach taken in this article is sufficient sampling for robust biexponential modeling and statistical evaluation of the resulting IVIM biomarkers. This work represents, to the authors’ knowledge, the first direct measurement and quantification of IVIM biomarkers of vascularity, cellularity, and blood velocity within breast tumors. Our conventional monoexponential ADC analysis is consistent with previous breast imaging studies [23,24,27,32,47,48] and distinguishes lesions from surrounding fibroglandular tissue according to the degree of restriction of the cellularity. However, some malignant lesions possess both high vascularity (high perfusion fraction and nonzero pseudodiffusion) and high cellularity (low tissue diffusivity), which influence the DWI signal decay in opposite directions, confounding diagnosis and grading by DWI. The compartmental analysis performed in this study is thus beneficial both for avoidance of systematic error and for enhanced quantification ability.

The results of the comparison of tissue types shown in Table 3 and Figure 7 illustrate biomarkers that can be used to distinguish lesions from normal fibroglandular tissue. Tissue diffusivity D_t shows stronger differentiation between normal and cancerous tissue (69.0 %) than does the ADC (58.5 %). The D_t parameter, by avoiding vascular contributions and marking cellularity more precisely, provides better differentiation of normal from IDC or OT lesions than does the ADC. The equivalence of ADC and D_t for normal fibroglandular tissue is consistent with a low microvascular volume fraction in FGT and an essentially undetectable IVIM effect there, consistent with the findings of Baron et.al.[31] Furthermore, within the lesion group, the most aggressive invasive ductal carcinoma group shows the highest cellularity (lower D_t), highest vascularity (higher f_p), and slowest blood velocity (lower D_p). Although this preliminary study had a small sample size, these results suggest the potential for lesion classification or monitoring of a given lesion over time via the IVIM parameter set that future studies might investigate.

The values shown in Table 3 and Figure 7 for the IDC lesion perfusion fraction f_p (f_p = 9.8 +/− 4.8 %) may be compared with those reported from other *in vivo* tumors, including implanted R3230 adenocarcima (f_p = 12.7 +/− 1.1 %) [49] and human hepatocellular carcinoma (f_p = 15 +/− 7%) [2], showing similar results.

The preliminary comparison with perfusion-weighted imaging revealed only modest correlation between analogous blood volume parameters (f_p and initial enhancement) but this is not surprising given the coarse temporal sampling of the perfusion imaging examination. Also, the timescales of the IVIM and perfusion examination are considerably different, and it is expected that IVIM provides more purely intravascular information than the longer timescale perfusion scan that includes extravasation. It is also noteworthy that the clinical evaluation of contrast enhancement kinetics (type 1, 2, or 3) did not segment the IDC lesions from the overall group, underscoring the potential benefit of the additional diffusion metrics of this study for lesion differentiation.

The spatially resolved IVIM analysis presented in Figure 6 for the case of a large tumor provides textural detail on the cellular/vascular biomarkers D_p, f_p and D_t. Also, the cross-correlation histograms provide another means to interpret their inter-relationships. In particular, the slight negative correlation observed between perfusion fraction (f_p) and the diffusivities D_p and D_t is consistent with a typical tumor microenvironment. Namely, abundant angiogenic neovascularity (high f_p) with sluggish flow (low D_p) occurs in tandem with proliferating cellularity (low D_t). The spatial mapping and image cross-correlations exemplified here may potentially be used to (a) characterize heterogeneity, (b) assess infiltration, and (c) guide targeted biopsies or drug delivery.

Limitations to our study include the inability to perform DWI on lesions < 1 cm. Our cohort was also biased with a large number of malignancies, and the benign lesions in our cohort were generally too small to be directly sampled in our diffusion images; future sequence / analysis development may address this limitation. We also employed only one diffusion sensitizing gradient orientation, limiting sensitivity to diffusion anisotropy. Since the vascular microstructure in malignant tumors is not expected to display a collective orientation pattern we do not expect diffusion anisotropy to play a strong role in their IVIM response; future work may investigate this possibility, however. The diffusion-weighting scheme employed more b-values than the absolute minimum required (4 for all 3 IVIM parameters) in keeping with the goals of exploring feasibility of measuring IVIM parameters as well as obtaining preliminary estimates in patient groups. However, the protocol could be abbreviated (to as few as 3 b-values for estimating D_t and f_p) if required by time constraints. Despite these limitations, we note that the ADC findings are consistent with recently published data on breast lesion DWI [23,24,27,32,47,48], and the IVIM parameter findings represent new biomarkers in breast lesions with great potential for tumor assessment, grading, and/or treatment monitoring in future studies.

V. CONCLUSIONS

The present study has measured quantitative IVIM biomarkers in patients with breast cancer. DWI response curves in lesions were found to be biexponential in comparison with the

monoexponential response in normal fibroglandular tissue. Quantification of perfusion fraction (f_p), tissue diffusivity (D_t), and pseudodiffusivity (D_p) provides noninvasive sensitivity to microenvironment properties without need of contrast agent and may have a role in screening breast MRI in high risk women. These applications have the potential to improve the specificity of breast MRI. Further work in a larger patient population and comparison with quantitative histology may demonstrate diagnostic ability for differentiation of lesions of variable malignancies (e.g. DCIS, adenocarcinoma, IDC). These tools are expected to enhance the role of MRI in diagnosis, monitoring, and treatment management of cancerous lesions in the breast, and perhaps provide surrogate markers of biological properties key to effective treatment.

ACKNOWLEDGMENTS

JDG was supported in part by a National Institutes of Health grant: NYUCI CCSG NIH/NCI P30 CA 16087.

REFERENCES

1. Jellison BJ, Field AS, Medow J, Lazar M, Salamat MS, Alexander AL. Diffusion Tensor Imaging of Cerebral White Matter: A Pictorial Review of Physics, Fiber Tract Anatomy, and Tumor Imaging Patterns. AJNR Am J Neuroradiol. 2004; 25(3):356–369. [PubMed: 15037456]
2. Yamada I, Aung W, Himeno Y, Nakagawa T, Shibuya H. Diffusion Coefficients in Abdominal Organs and Hepatic Lesions: Evaluation with Intravoxel Incoherent Motion Echo-planar MR Imaging. Radiology. 1999; 210(3):617–623. [PubMed: 10207458]
3. Squillaci E, Manenti G, Cova M, Di Roma M, Miano R, Palmieri G, Simonetti G. Correlation of diffusion-weighted MR imaging with cellularity of renal tumours. Anticancer Research. 2004; 24(6):4175–4179. [PubMed: 15736469]
4. McVeigh PZ, Syed AM, Milosevic M, Fyles A, Haider MA. Diffusion-weighted MRI in cervical cancer. European Radiology. 2008; 18(5):1058–1064. [PubMed: 18193428]
5. Sinha S, Sinha U. Functional magnetic resonance of human breast tumors - Diffusion and perfusion imaging. Techniques in Bioinformatics and Medical Informatics. 2002; 980:95–115.
6. Mulkern RV, Barnes AS, Haker SJ, Hung YP, Rybicki FJ, Maier SE, Tempany CMC. Biexponential characterization of prostate tissue water diffusion decay curves over an extended b-factor range. Magnetic Resonance Imaging. 2006; 24(5):563–568. [PubMed: 16735177]
7. Dudeck O, Zeile M, Pink D, Pech M, Tunn PU, Reichardt P, Ludwig WD, Hamm B. Diffusion-weighted magnetic resonance imaging allows monitoring of anticancer treatment effects in patients with soft-tissue sarcomas. Journal of Magnetic Resonance Imaging. 2008; 27(5):1109–1113. [PubMed: 18425832]
8. Lee KC, Bradley DA, Hussain M, Meyer CR, Chenevert TL, Jacobson JA, Johnson TD, Galban CJ, Rehemtulla A, Pienta KJ, Ross BD. A feasibility study evaluating the functional diffusion map as a predictive imaging biomarker for detection of treatment response in a patient with metastatic prostate cancer to the bone. Neoplasia. 2007; 9(12):1003–1011. [PubMed: 18084607]
9. Baehring JM, Bi WYL, Bannykh S, Piepmeier JM, Fulbright RK. Diffusion MRI in the early diagnosis of malignant glioma. Journal of Neuro-Oncology. 2007; 82(2):221–225. [PubMed: 17029014]
10. Stadlbauer A, Nimsky C, Gruber S, Moser E, Hammen T, Engelhorn T, Buchfelder M, Ganslandt O. Changes in fiber integrity, diffusivity, and metabolism of the pyramidal tract adjacent to gliomas: A quantitative diffusion tensor fiber tracking and MR spectroscopic imaging study. American Journal of Neuroradiology. 2007; 28(3):462–469. [PubMed: 17353313]
11. Kim S, Pickup S, Hsu O, Poptan iH. Diffusion tensor MRI in rat models of invasive and well-demarcated brain tumors. NMR in Biomedicine. 2008; 21(3):208–216. [PubMed: 17530617]

12. Zhang JY, van Zijl PCM, Laterra J, Salhotra A, Lal B, Mori S, Zhou JY. Unique patterns of diffusion directionality in rat brain tumors revealed by high-resolution diffusion tensor MRI. Magnetic Resonance in Medicine. 2007; 58(3):454–462. [PubMed: 17763344]
13. Tropine A, Dellani PD, Glaser M, Bohl J, Ploner T, Vucurevic G, Perneczky A, Stoeter P. Differentiation of fibroblastic meningiomas from other benign subtypes using diffusion tensor imaging. Journal of Magnetic Resonance Imaging. 2007; 25(4):703–708. [PubMed: 17345634]
14. Wu JS, Mao Y, Zhou LF, Tang WJ, Hu J, Song YY, Hong XN, Du GH. Clinical evaluation and follow-up outcome of diffusion tensor IMAGING-BASED functional neuronavigation: A prospective, controlled study in patients with gliomas involving pyramidal tracts. Neurosurgery. 2007; 61(5):935–948. [PubMed: 18091270]
15. Le Bihan D, Breton E, Lallemand D, Grenier P, Cabanis E, Laval-Jeantet M. MR imaging of intravoxel incoherent motions: application to diffusion and perfusion in neurologic disorders. Radiology. 1986; 161(2):401–407. [PubMed: 3763909]
16. Le Bihan D, Breton E, Lallemand D, Aubin M, Vignaud J, Laval-Jeantet M. Separation of diffusion and perfusion in intravoxel incoherent motion MR imaging. Radiology. 1988; 168(2): 497–505. [PubMed: 3393671]
17. Lebihan D, Breton E, Lallemand D, Desbleds MT, Aubin ML, Vignaud J, Roger B. Contribution of Intravoxel Incoherent Motion (Ivim) Imaging to Neuroradiology. J Neuroradiology. 1987; 14(4):295–312.
18. Le Bihan D. Intravoxel Incoherent Motion Perfusion MR Imaging: A Wake-Up Call. Radiology. 2008; 249(3):748–752. [PubMed: 19011179]
19. Luciani A, Vignaud A, Cavet M, Tran Van Nhieu J, Mallat A, Ruel L, Laurent A, Deux J-F, Brugieres P, Rahmouni A. Liver Cirrhosis: Intravoxel Incoherent Motion MR Imaging--Pilot Study. Radiology. 2008; 249(3):891–899. [PubMed: 19011186]
20. Callot V, Bennett E, Decking UKM, Balaban RS, Wen H. In vivo study of microcirculation in canine myocardium using the IVIM method. Magnetic Resonance in Medicine. 2003; 50(3):531–540. [PubMed: 12939761]
21. Wang Z, Su M-Y, Nalcioglu O. Measurement of tumor vascular volume and mean microvascular random flow velocity magnitude by dynamic GD-DTPA-Albumin enhanced and diffusion-weighted MRI. Magnetic Resonance in Medicine. 1998; 40(3):397–404. [PubMed: 9727942]
22. Wang Z, Su M-Y, Najafi A, Nalcioglu O. Effect of vasodilator hydralazine on tumor microvascular random flow and blood volume as measured by intravoxel incoherent motion (IVIM) weighted MRI in conjunction with Gd-DTPA-Albumin enhanced MRI. Magnetic Resonance Imaging. 2001; 19(8):1063–1072. [PubMed: 11711230]
23. Sinha S, Lucas-Quesada FA, Sinha U, DeBruhl N, Bassett LW. In vivo diffusion-weighted MRI of the breast: Potential for lesion characterization. Journal of Magnetic Resonance Imaging. 2002; 15(6):693–704. [PubMed: 12112520]
24. Sharma U, Danishad KKA, Seenu V, Jagannathan NR. Longitudinal study of the assessment by MRI and diffusion-weighted imaging of tumor response in patients with locally advanced breast cancer undergoing neoadjuvant chemotherapy. Nmr in Biomedicine. 2009; 22(1):104–113. [PubMed: 18384182]
25. Yankeelov TE, Lepage M, Chakravarthy A, Broome EE, Niermann KJ, Kelley MC, Meszoely I, Mayer IA, Herman CR, McManus K, Price RR, Gore JC. Integration of quantitative DCE-MRI and ADC mapping to monitor treatment response in human breast cancer: initial results. Magnetic Resonance Imaging. 2007; 25(1):1–13. [PubMed: 17222711]
26. Paran Y, Bendel P, Margalit R, Degani H. Water diffusion in the different microenvironments of breast cancer. Nmr in Biomedicine. 2004; 17(4):170–180. [PubMed: 15229930]
27. Bogner W, Gruber S, Pinker K, Grabner G, Stadlbauer A, Weber M, Moser E, Helbich TH, Trattnig S. Diffusion-weighted MR for Differentiation of Breast Lesions at 3.0 T: How Does Selection of Diffusion Protocols Affect Diagnosis? Radiology. 2009; 253(2):341–351. [PubMed: 19703869]
28. Peters, N.; Vincken, K.; van den Bosch, M.; Luijten, P.; Mali, W.; Bartels, L. Proc. ISMRM. Honolulu: Apr. 2009 Quantitative DWI for differentiation of benign and malignant breast lesions: the influence of the choice of b-values.; p. 582

29. Yuen, S.; Goto, M.; Yamada, K.; Takahata, A.; Nishida, K.; Nishimura, T. Proc. ISMRM. Honolulu: Apr. 2009 Microperfusion-induced Elevation of ADC is Suppressed after Contrast in Breast Carcinoma.; p. 4233
30. Zhang, J.; Cheng, L.; Guo, Y.; Sun, F. Proc. ISMRM. Honolulu: Apr. 2009 The optimized b value of Breast Diffusion Weighted MRI.; p. 2101
31. Baron P, Dorrius MD, Kappert P, Oudkerk M, Sijens PE. Diffusion-weighted imaging of normal fibroglandular breast tissue: influence of microperfusion and fat suppression technique on the apparent diffusion coefficient. Nmr in Biomedicine. 2010; 23(4):399–405. [PubMed: 20131313]
32. Partridge SC, DeMartini WB, Kurland BF, Eby PR, White SW, Lehman CD. Differential diagnosis of mammographically and clinically occult breast lesions on diffusion-weighted MRI. Journal of Magnetic Resonance Imaging. 2010; 31(3):562–570. [PubMed: 20187198]
33. Vincensini D, Dedieu V, Eliat PA, Vincent C, Bailly C, de Certaines J, Joffre F. Magnetic resonance imaging measurements of vascular permeability and extracellular volume fraction of breast tumors by dynamic Gd-DTPA-enhanced relaxometry. Magnetic Resonance Imaging. 2007; 25(3):293–302. [PubMed: 17371717]
34. Eyal E, Degani H. Model-based and model-free parametric analysis of breast dynamic-contrast-enhanced MRI. Nmr in Biomedicine. 2009; 22(1):40–53. [PubMed: 18022997]
35. Huang W, Li X, Morris EA, Tudorica LA, Seshan VE, Rooney WD, Tagge I, Wang Y, Xu J, Springer CS. The magnetic resonance shutter speed discriminates vascular properties of malignant and benign breast tumors in vivo. Proceedings of the National Academy of Sciences. 2008; 105(46):17943–17948.
36. Li X, Huang W, Morris EA, Tudorica LA, Seshan VE, Rooney WD, Tagge I, Wang Y, Xu J, Springer CS. Dynamic NMR effects in breast cancer dynamic-contrast-enhanced MRI. Proceedings of the National Academy of Sciences. 2008; 105(46):17937–17942.
37. Bastin ME, Le Roux P. On the application of a non-CPMG single-shot fast spin-echo sequence to diffusion tensor MRI of the human brain. Magnetic Resonance in Medicine. 2002; 48(1):6–14. [PubMed: 12111926]
38. Carballido-Gamio J, Xu D, Newitt D, Han ET, Vigneron DB, Majumdar S. Single-shot fast spin-echo diffusion tensor imaging of the lumbar spine at 1.5 and 3 T. Magnetic Resonance Imaging. 2007; 25(5):665–670. [PubMed: 17540278]
39. Kinoshita T, Yashiro N, Ihara N, Funatu H, Fukuma E, Narita M. Diffusion-weighted half-fourier single-shot turbo spin echo imaging in breast tumors: Differentiation of invasive ductal carcinoma from fibroadenoma. Journal of Computer Assisted Tomography. 2002; 26(6):1042–1046. [PubMed: 12488758]
40. ACR. American College of Radiology Breast Imaging Reporting and Data System (BI RADS). American College of Radiology; 2003.
41. Wirestam R, Borg M, Brockstedt S, Lindgren A, Holtas S, Stahlberg F. Perfusion-related parameters in intravoxel incoherent motion MR imaging compared with CBV and CBF measured by dynamic susceptibility-contrast MR technique. Acta Radiologica. 2001; 42(2):123–128. [PubMed: 11281143]
42. Moteki T, Horikoshi H. Evaluation of hepatic lesions and hepatic parenchyma using diffusion-weighted echo-planar MR with three values of gradient b-factor. Journal of Magnetic Resonance Imaging. 2006; 24(3):637–645. [PubMed: 16888790]
43. Yao L, Sinha U. Imaging the microcirculatory proton fraction of muscle with diffusion-weighted echo-planar imaging. Acad Radiol. 2000; 7(1):27–32. [PubMed: 10645455]
44. Zhang JL, Sigmund EE, Chandarana H, Rusinek H, Chen Q, Vivier P-H, Taouli B, Lee VS. Variability of Renal Apparent Diffusion Coefficients: Limitations of the Monoexponential Model for Diffusion Quantification. Radiology. 2010; 254(3):783–792. [PubMed: 20089719]
45. Taouli B, Tolia AJ, Losada M, Babb JS, Chan ES, Bannan MA, Tobias H. Diffusion-weighted MRI for quantification of liver fibrosis: Preliminary experience. Am J Roentgenol. 2007; 189(4): 799–806. [PubMed: 17885048]
46. Taouli B, Vilgrain V, Dumont E, Daire JL, Fan B, Menu Y. Evaluation of liver diffusion isotropy and characterization of focal hepatic lesions with two single-shot echo-planar MR imaging sequences: Prospective study in 66 patients. Radiology. 2003; 226(1):71–78. [PubMed: 12511671]

47. Woodhams R, Kakita S, Hata H, Iwabuchi K, Kuranami M, Gautam S, Hatabu H, Kan S, Mountford C. Identification of Residual Breast Carcinoma Following Neoadjuvant Chemotherapy: Diffusion-weighted Imaging--Comparison with Contrast-enhanced MR Imaging and Pathologic Findings. Radiology. 2010; 254(2):357–366. [PubMed: 20093508]

48. Lo GG, Ai V, Chan JKF, Li KW, Cheung PSY, Wong TT, Ma M, Lee R, Chien D. Diffusion-Weighted Magnetic Resonance Imaging of Breast Lesions: First Experiences at 3 T. Journal of Computer Assisted Tomography. 2009; 33(1):63–69. [PubMed: 19188787]

49. Wang ZH, Su MY, Najafi A, Nalcioglu O. Effect of vasodilator hydralazine on tumor microvascular random flow and blood volume as measured by intravoxel incoherent motion (IVIM) weighted MRI in conjunction with Gd-DTPA-Albumin enhanced MRI. Magnetic Resonance Imaging. 2001; 19(8):1063–1072. [PubMed: 11711230]

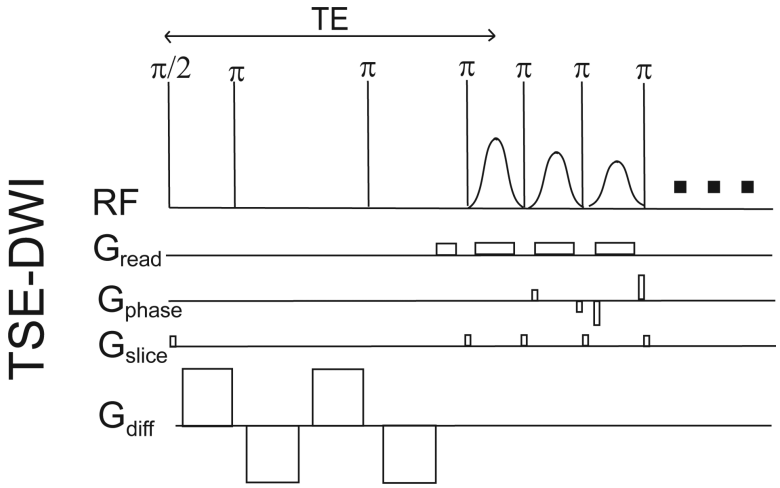

Figure 1.
Single shot turbo spin echo (TSE) – DWI sequence with twice refocused bipolar gradient diffusion preparation.

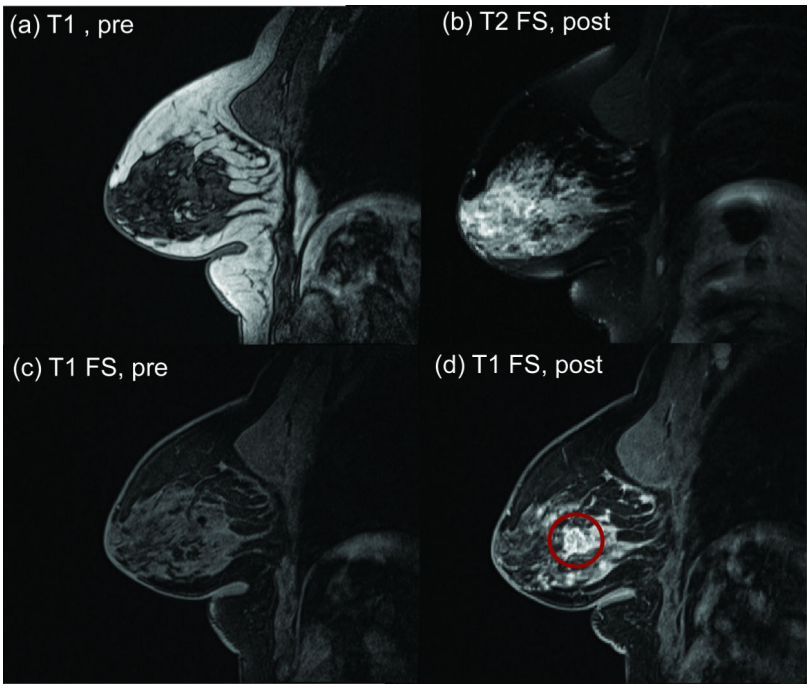

Figure 2.
Sagittal anatomical images of breast lesion (red circle) before and after contrast administration. (a) Pre-contrast T1 VIBE. (b) Post-contrast T2-weighted fat-saturated image. (c) Pre-contrast T1-weighted fat-saturated image. (d) Post-contrast T1-weighted fat-saturated image.

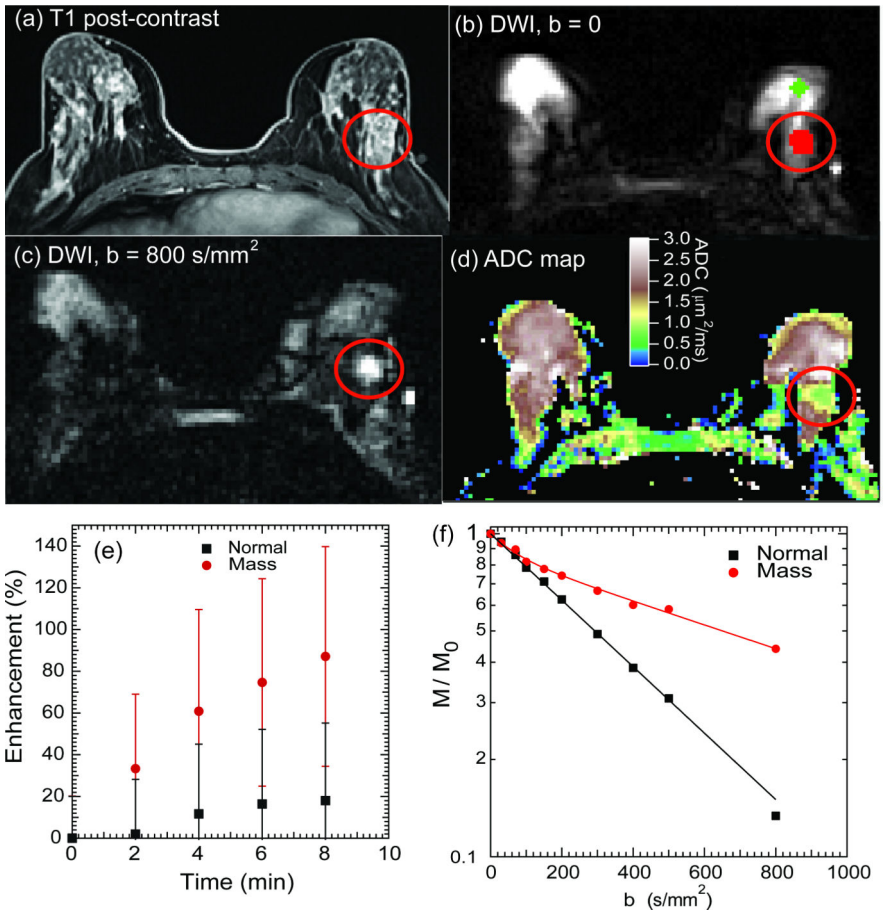

Figure 3.

Breast cancer (LABC) IVIM-MRI results at 3 T. (a) Gd-DTPA contrast enhanced T1-weighted axial image showing left breast invasive ductal carcinoma (IDC) lesion (red circles). (b) Unweighted (b= 0) axial DWI and regions of interest for normal tissue (green) and lesion (red). (c) Axial DWI, b = 800 s/mm^2, where lesion appears hyperintense due to cellularity-induced restricted diffusion. (d) ADC map showing lower apparent diffusion in lesion area.(e) Relative contrast enhancement curves for normal fibroglandular tissue and mass region. (f) DWI signal intensity decays for normal FG tissue and mass region. The mass region demonstrates both restricted diffusion and fast vascular pseudodiffusion.

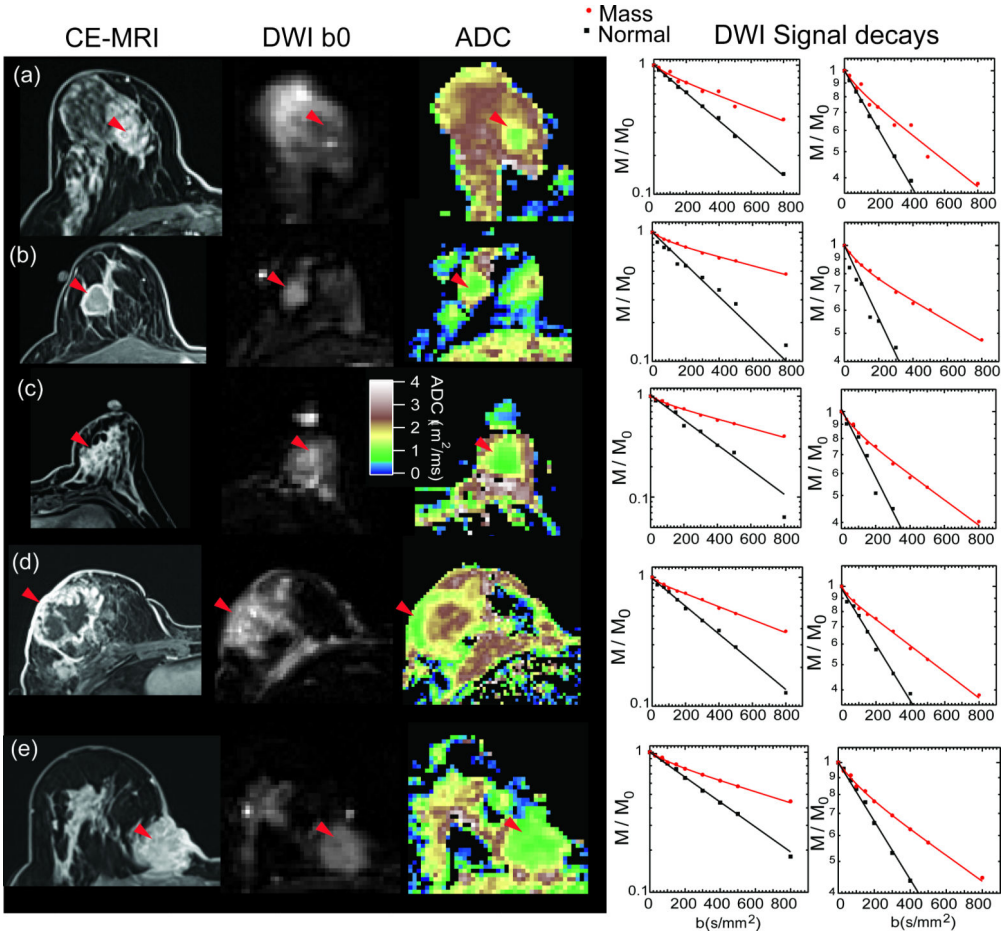

Figure 4.

Example results from several patients in this study. (a) DCIS lesion; (b)-(e) IDC lesions. From left to right: Post-contrast T1 images showing lesion location (red arrowheads); DWI unweighted (b0) images in which lesion is also hyperintense; ADC map showing lower values in lesions than in FG tissue; DWI signal intensity profiles from the lesion area and normal tissue. The enlarged scale view highlights the nonexponential response of the lesion tissue in comparison with the monoexponential behavior of FG tissue.

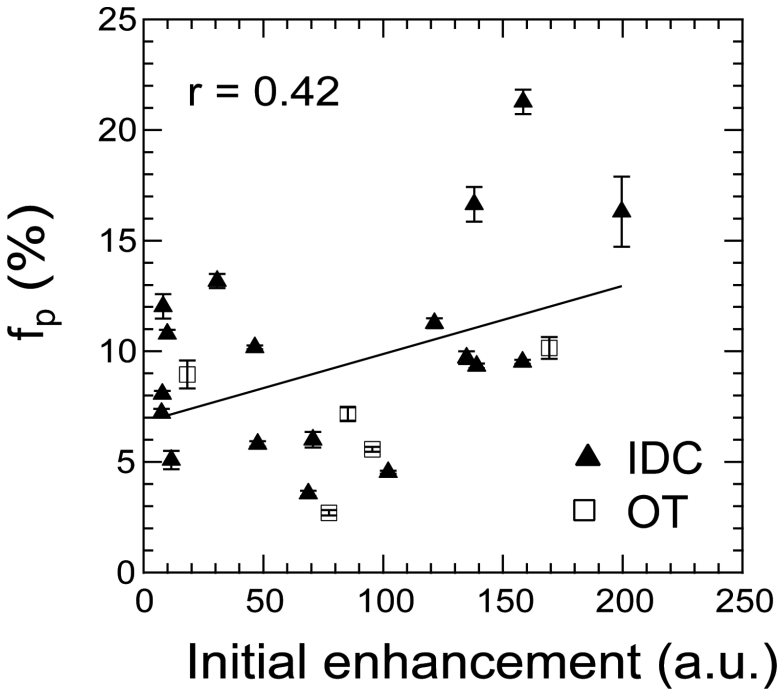

Figure 5.
Correlation of f_p with CE-MRI initial enhancement. The correlation coefficient amongst all lesions (solid line) is r = 0.42.

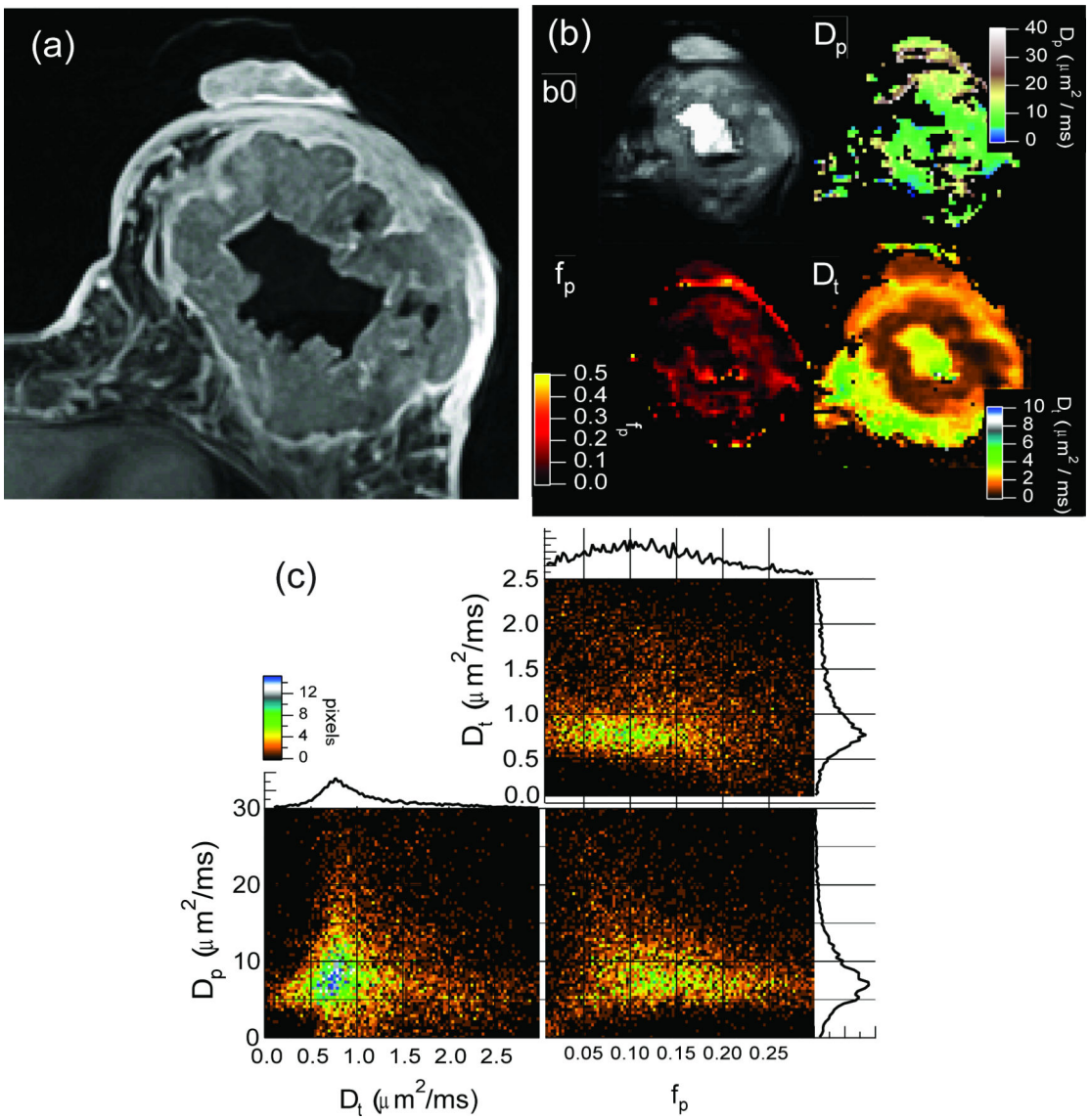

Figure 6.

(a) Contrast-enhanced MRI of a breast tumor. (b) DWI unweighted image (b0) and IVIM parametric maps of f_p, D_p, and D_t. (c) Two-dimensional histogram cross-correlations between IVIM parameters (f_p, D_p, and D_t) in tumor regions from whole-breast acquisition. The slight negative correlation observed between perfusion fraction (f_p) and the diffusivities D_p and D_t is consistent with a typical tumor microenvironment, in which abundant angiogenic neovascularity (high f_p) with sluggish flow (low D_p) occurs in tandem with proliferating cellularity (low D_t).

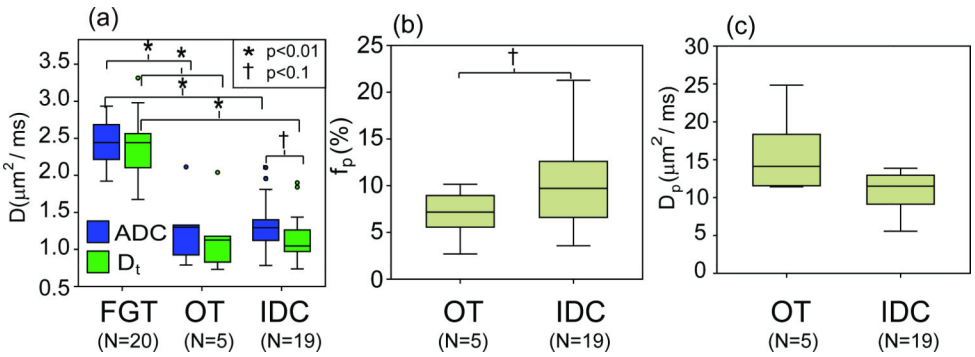

Figure 7.

Breast patient group analysis for IVIM parameters (a) ADC and D_t, (b) f_p, and (c) D_p. FGT = normal fibroglandular tissue, IDC = invasive ductal carcinoma, OT = other malignant lesions.

Table 1

Lesion distribution considered in this study.

	LCIS	ILC	DCIS	Adeno	IDC	Total
All w/pathology	1	3	4	1	35	44
size > 10 mm	0	2	2	1	19	24

LCIS = lobular carcinoma in situ, ILC = invasive lobular carcinoma, DCIS = ductal carcinoma in situ, adeno = adenocarcinoma, IDC = invasive ductal carcinoma.

Table 2

Pearson correlation coefficients (r) between IVIM parameters and initial contrast enhancement in breast lesions.

	IDC lesions (N=18)	All lesions (N=23)
ADC	−0.14	−0.12
D_t	−0.35	−0.27
f_p	0.48	0.42
D_p	−0.32	−0.24

Table 3

Summary of groups (mean value ± standard deviation) from IVIM analysis of DWI ROI data in the cohort of breast patients.

	Normal FGT (n=20)	All lesions (n=24)	Δ(%) FGT/ all	* p FGT/ all	IDC (n=19)	Δ(%) FGT/ IDC	* p FGT/ IDC	OT (n=5)	Δ(%) FGT/ OT	* p FGT/ OT	Δ(%) IDC/ OT	* p IDC/ OT
ADC (μ,m^2/ms)	2.44±0.30	1.34 ± 0.39	58.5	<0.01	1.35±0.36	57.1	<0.01	1.29 ± 0.52	61.6	<0.01	4.2	0.83
D_t (μ,m^2/ms)	2.36±0.38	1.15 ± 0.35	69.0	<0.01	1.14±0.32	68.8	<0.01	1.18 ± 0.52	66.7	<0.01	−3.3	0.88
f_p (%)	N.A.	9.8 ± 4.8	N.A.	N.A.	10.5±5.0	N.A.	N.A.	6.9 ± 2.9	N.A.	N.A.	41.4	0.06
D_p (μm^2/ms)	N.A.	15.1 ± 10.4	N.A.	N.A.	14.9 ± 11.4	N.A.	N.A.	16.1 ± 5.7	N.A.	N.A.	−7.5	0.75

Diffusion parameters are compared between normal fibroglandular tissue (FGT) and lesion groups (all, IDC, OT) via 2 sided t-tests. Within the lesion group, the subtypes invasive ductal carcinoma (IDC) and other malignant (OT) lesions are compared in the same way. Note that quantification of the perfusion parameters f_p and D_p is only possible within lesions. Percent differences (Δ) are also shown for each group comparison.

*p-value reflects test of mean differences between groups using paired or unpaired t-tests as appropriate (see text).